Cellular/Molecular

An Essential Role for Modulation of Hyperpolarization-Activated Current in the Development of Binaural Temporal Precision

Sukant Khurana,[1] Zhiqiang Liu,[2] Alan S. Lewis,[2] Kristen Rosa,[1] Dane Chetkovich,[2,3] and Nace L. Golding[1]

[1]Section of Neurobiology and Institute for Neuroscience, University of Texas at Austin, Austin, Texas 78712, [2]Davee Department of Neurology and Clinical Neurosciences and [3]Department of Physiology, Feinberg School of Medicine, Northwestern University, Chicago, Illinois 60611

In sensory circuits of the brain, developmental changes in the expression and modulation of voltage-gated ion channels are a common occurrence, but such changes are often difficult to assign to clear functional roles. We have explored this issue in the binaural neurons of the medial superior olive (MSO), whose temporal precision in detecting the coincidence of binaural inputs dictates the resolution of azimuthal sound localization. We show that in MSO principal neurons of gerbils during the first week of hearing, a hyperpolarization-activated current (I_h) progressively undergoes a 13-fold increase in maximal conductance, a >10-fold acceleration of kinetics, and, most surprisingly, a 30 mV depolarizing shift in the voltage dependence of activation. This period is associated with an upregulation of the hyperpolarization-activated and cyclic nucleotide-gated (HCN) channel subunits HCN1, HCN2, and HCN4 in the MSO, but only HCN1 and HCN4 were expressed strongly in principal neurons. I_h recorded in nucleated patches from electrophysiologically mature MSO neurons (>P18) exhibited kinetics and an activation range nearly identical to the I_h found in whole-cell recordings before hearing onset. These results indicate that the developmental changes in I_h in MSO neurons can be explained predominantly by modulation from diffusible intracellular factors, and not changes in channel subunit composition. The exceptionally large modulatory changes in I_h, together with refinements in synaptic properties transform the coding strategy from one of summation and integration to the submillisecond coincidence detection known to be required for transmission of sound localization cues.

Introduction

Hyperpolarization-activated and cyclic nucleotide-gated (HCN) channels are cation-selective channels that subserve critical functions in both neurons and cardiac myocytes (for reviews, see (DiFrancesco, 1993; Robinson and Siegelbaum, 2003). In mammals these channels consist of homo- or heterotetrameric subunits encoded by four genes, *HCN1–HCN4* (Ludwig et al., 1998; Santoro et al., 1998; Seifert et al., 1999). The presence and relative abundance of each subunit in each channel influences both the voltage dependence of the channel as well as its kinetics (Santoro et al., 2000). The activation of these channels in the subthreshold voltage range provides a non-inactivating inward current (I_h) that typically influences the value of the resting potential. In addition, the dynamic activation and deactivation of I_h during network activity and the resulting interactions with other voltage-gated channels can shape the amplitude and time course of synaptic potentials (Stuart and Spruston, 1998; Magee, 1999; Khurana et al., 2011), and in some instances promote pacemaking and other rhythmic firing patterns (McCormick and Pape, 1990; Zolles et al., 2006).

In central auditory neurons, HCN channels play a fundamental role in coding temporal information, information that is in turn used for localizing sounds and understanding speech and communication signals. The coexpression of HCN channels and *KCNA1* (K_v1) potassium channels appears as a common motif in several classes of brainstem auditory neurons, conferring a large resting conductance that reduces the membrane time constant and improves the fidelity with which these neurons signal the timing of their excitatory inputs (Golding et al., 1995; Bal and Oertel, 2000; Leao et al., 2006; Hassfurth et al., 2009; Khurana et al., 2011). Many of the biophysical adaptations for precise temporal coding are not present in auditory neurons at birth, but instead develop progressively during early postnatal development, giving rise to changes in synaptic and intrinsic temporal precision of over two orders of magnitude (Svirskis et al., 2002; Magnusson et al., 2005; Scott et al., 2005; Chirila et al., 2007). While the development of synapse structure and properties for precise auditory coding have been extensively investigated (Bellingham et al., 1998; Taschenberger and von Gersdorff, 2000; Brenowitz and Trussell, 2001; Joshi et al., 2004; Koike-Tani et al., 2008), the cellular mechanisms by which changes in voltage-gated ion channels shape auditory processing during early auditory development are less well understood.

Received July 28, 2011; revised Dec. 8, 2011; accepted Dec. 13, 2011.

Author contributions: S.K., Z.L., A.S.L., D.C., and N.L.G. designed research; S.K., Z.L., A.S.L., and K.R. performed research; S.K., Z.L., A.S.L., K.R., D.C., and N.L.G. analyzed data; S.K., D.C., and N.L.G. wrote the paper.

This work was supported by NIH Grants DC006788 (N.L.G.); NS064757 (A.S.L.); and NS05595 and NS059934 (D.M.C.). We thank Quratul-Ain Ismail for technical assistance, and Dr. Donata Oertel for comments on a previous version of the manuscript.

Correspondence should be addressed to Nace L. Golding, Section of Neurobiology and Center for Learning and Memory, University of Texas at Austin, 1 University Station, C0920, Austin TX 78712-0248. E-mail: golding@mail.utexas.edu.

DOI:10.1523/JNEUROSCI.3882-11.2012

 0270-6474/12/322814-10$15.00/0

We examined how developmental changes in HCN channels shape temporal coding in the principal neurons of the medial superior olive (MSO). These neurons convey cues for horizontal sound localization by detecting temporal correlations in the patterns of synaptic excitation driven by sounds from each ear ("binaural coincidence detection"), a computation requiring temporal resolution on a time scale of tens of microseconds. Using a combination of molecular, immunofluorescence, pharmacological, and electrophysiological approaches, we explore the developmental changes in I_h that take place around the onset of hearing, and demonstrate a pivotal role played by I_h modulation in conferring temporal precision to binaural coincidence detection.

Materials and Methods

All experimental procedures were approved by the University of Texas at Austin and Northwestern University Institutional Animal Care and Use Committees, following the guidelines of the National Institutes of Health.

Brainstem slice preparation

Mongolian gerbils (*Meriones unguiculatus*) of either sex were procured from Charles River Laboratories or bred at the Animal Resource Center of the University of Texas at Austin. Brainstem slices were prepared from animals between postnatal ages 6 and 30 d. Briefly, animals were decapitated under halothane anesthesia, and the brain removed in artificial CSF (ACSF) at 32°C composed of the following (in mM): 125 NaCl, 2.5 KCl, 2 $CaCl_2$, 20 $NaHCO_3$, 1.25 NaH_2PO_4, 25 glucose, and 1.0 $MgCl_2$, pH 7.45 with NaOH. Horizontal sections containing the superior olivary complex were cut at a thickness of 200 μm with an oscillating tissue slicer (VT1000S or 1200S; Leica), incubated at 35°C for 30–45 min, and then maintained at room temperature (24–25°C). MSO principal cells were visualized using contrast-enhanced differential interference contrast microscopy and selected according to previously determined criteria (Scott et al., 2005).

Electrophysiology

Voltage-clamp experiments. All electrophysiological recordings were conducted at 35°C in ACSF. Electrodes were pulled from borosilicate glass (1.65 OD; WPI), and had resistances of 4–6 MΩ in ACSF. Within this range of pipette sizes, average time-related changes in maximum conductance and activation [half-maximal activation voltage ($V_{1/2}$)] were <10% and 2 mV, respectively, before 30 min after break-in (data not shown), and all whole-cell measurements were restricted to this time window. For whole-cell recordings, the intracellular pipette solution contained the following (in mM): 127 potassium gluconate, 8 KCl, 10 sodium phosphocreatine, 10 HEPES, 0.5 EGTA, 4 MgATP, 0.3 NaGTP, pH 7.3, with KOH. I_h was pharmacologically isolated by including the following in the external ACSF as follows (in mM): 1 3,4-diaminopyridine (DiAP), 10 TEA-Cl, 0.2 4-AP, 0.2 $BaCl_2$, 0.001 TTX, 0.05 $NiCl_2$, 0.2 $CoCl_2$, 0.01 CNQX, 0.05 D-AP5, and 0.001 strychnine. To block I_h, 50 μM ZD7288 was added to the bath or 20 μM to the pipette solution. Blockers were obtained from Tocris Cookson except for strychnine, which was obtained from Sigma-Aldrich.

Nucleated patch recordings were obtained as in previous studies using the same pipette solution as whole-cell recordings (Sather et al., 1992; Scott et al., 2010). Patches were deemed stable and included in the dataset if the input resistance exceeded 700 MΩ (measured in voltage-clamp using a 3–6 mV step from a holding potential of −60 mV). Cell-attached patch-clamp recordings were made using a pipette solution of the following (in mM): 132.5 KCl, 2.5 NaCl, 10 HEPES, 1 EGTA, 2 $MgCl_2$, 2 DiAP, 0.001 TTX, 0.6 $BaCl_2$, and 1 $CaCl_2$.

All voltage-clamp recordings were made with an Axopatch 200B (Molecular Devices), filtered at 1 kHz, digitized at 50 kHz and acquired to computer using an Instrutech ITC-18 interface (HEKA Instruments) in conjunction with custom macros programmed in IgorPro (WaveMetrics). For all voltage-clamp experiments, electrodes were insulated with Parafilm to reduce capacitance, and series resistance and capacitance were compensated by at least 85%. All data from whole-cell and nucleated patches are plotted after correction for a liquid junction potential of 10 mV.

Current-clamp experiments. For whole-cell current-clamp recordings, the pipette solution was identical to that of voltage-clamp experiments (described above). Recordings were made with a BVC-700A amplifier (Dagan Corp). Electrode capacitance and series resistance were fully compensated. MSO neuron recordings were included in the dataset if they exhibited series resistances <15 MΩ and resting potentials below −55 mV. Data were low-pass filtered at 5 kHz and acquired to computer at 50 kHz as in voltage-clamp experiments. All data are plotted after correction for a liquid junction potential of 10 mV. For coincidence detection experiments, glutamatergic inputs were isolated through the addition of strychnine (1 μM). Stimulation of ipsilateral and contralateral inputs was adjusted to the lowest level that triggered consistent action potential firing when the peaks of the EPSPs were temporally aligned [defined as 0 μs interaural time difference (ITD)]. Stimuli were then offset in 100 μs increments, up to values as high as 1200 μs, depending on conditions. Under different pharmacological conditions (e.g., blockade of I_h by ZD7288), responses to synaptic stimuli changed in amplitude due to alterations in the input resistance of cell. Stimulation amplitude was thus readjusted to the lowest level that elicited consistent action potential firing at 0 μs ITD. Action potential probability was calculated from 10 to 20 responses, the value of which was uniform within each experiment.

Modulators of HCN channels

All modulators were purchased from Tocris Bioscience unless otherwise indicated. Wortmannin, a cell-permeable and irreversible inhibitor of phosphatidylinositol 3-kinase that depletes phosphatidylinositol-4,5-bisphosphate (PIP_2), was dissolved in DMSO to make 20 mM stock aliquots. SB203580 hydrochloride, a selective inhibitor of p38 mitogen-activated protein (MAP) kinase, was dissolved in water to make 10 mM stock aliquots. Sodium dibutyryl-cAMP (dB-cAMP), a membrane permeable analog of cAMP, was dissolved in water to make 100 mM aliquots. Forskolin, a cell-permeable activator of adenylyl cyclase that increases the levels of cAMP in cells was dissolved in DMSO to make 25 mM stock aliquots. All stock aliquots were used only once, within 3 months of preparation, and were stored at −20°C. The final concentration of these agents (20 μM wortmannin, 10 μM SB203580, 300 μM dB-cAMP, and 100 μM forskolin) was obtained by dissolving the stock solution in ACSF. Whenever the solvent was different from water, control solutions contained an identical concentration of vehicle alone.

In some experiments dB-cAMP (300 μM) and disodium salt of PIP_2 (100 μM) were added to pipette solutions and used as intracellular modulators. Intracellular solutions containing dB-cAMP, PIP_2, or both were stored at −20°C. Before use, the PIP_2-containing intracellular solution was sonicated for 30 min to ensure full dissolution of PIP_2. PIP_2 (≥98% purity) from bovine brain extract was obtained from Sigma-Aldrich.

Data analyses

Current-clamp. All analyses were performed using IgorPro. For current-clamp studies peak and steady-state voltage–current (V–I) plots were generated from voltage responses to 100 or 200 ms current steps measured at the peak and during the last 10 ms of the step pulse, respectively. The input resistance was obtained from the slope of the peak V–I relationship between 0 and 10 mV below rest.

Voltage-clamp. MSO neurons were held at −60 mV, and then stepped to −30 mV for 0.5–1.0 s to deactivate I_h. Subsequently, I_h was activated with steps (1–2 s duration) from −30 to −120 mV in 10 mV increments. Peak tail currents were averaged from the 5 ms immediately after the capacitive transient, normalized to the maximum currents obtained after the most negative prepulse (either −110 or −120 mV) and then plotted as a function of step potential. For measurements of whole-cell conductance, holding and instantaneous leak currents were subtracted from total current, and chord conductance was calculated according to the equation: $G_{h(max)} = I_h/(V_m - E_h)$, where $G_{h(max)}$ is the maximal conductance, V_m is the membrane potential, and E_h is the experimentally determined reversal potential of I_h (−38 mV) (Khurana et al., 2011). The G/G_{max} relation was well fitted by the Boltzmann function, of the form: $f(V) = 1/(1 + \exp[(V_{1/2} - V)/k])$, where V is the membrane voltage and

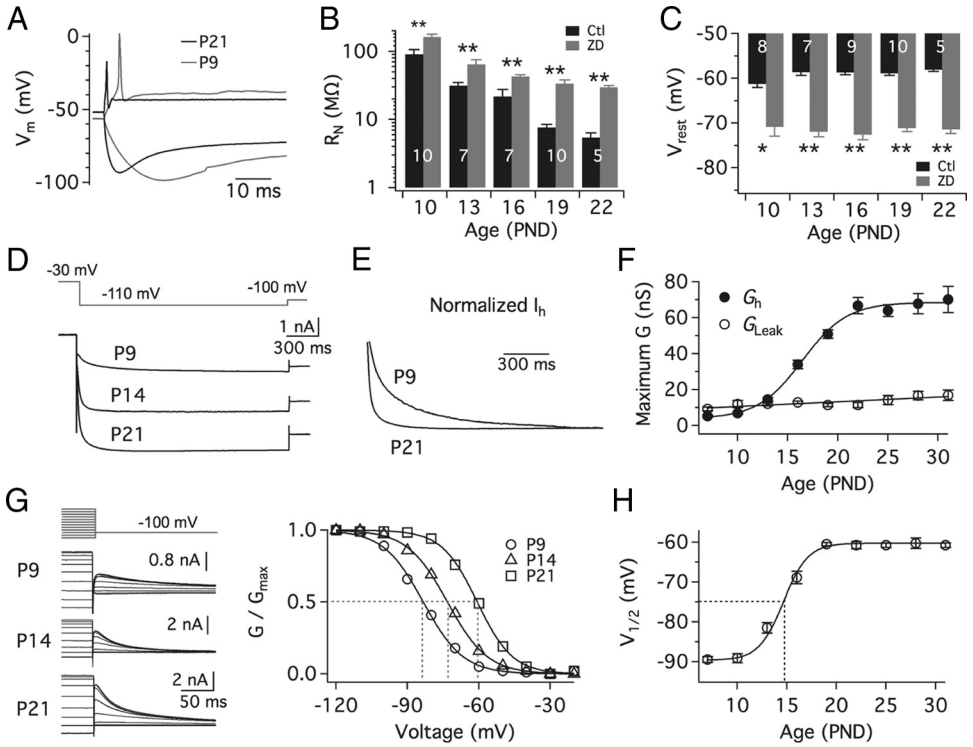

Figure 1. Maturation of I_h during the first week of hearing. ***A***, Response of an MSO principal neuron to both depolarizing and hyperpolarizing current injection before and ~1 week after hearing onset (P9 and P21, respectively). Mature MSO neurons exhibit faster membrane time constants and small action potentials. ***B***, Steady-state input resistance (R_N) of MSO neurons decreases with age, while the fractional contribution of I_h to the steady-state input resistance increased from 80% to 400% during auditory maturation. Data were binned in 3 d intervals centered on the age indicated. $^{**}p < 0.01$, two-tailed, paired *t* test. ***C***, Blockade of I_h at all ages hyperpolarized the resting potential by 9–14 mV. Binning and statistics as in ***B***. ***D***, Whole-cell voltage-clamp measurements of I_h show an increase during development. Traces are aligned by the current at −30 mV. ***E***, The speed of I_h kinetics increased during the first week of hearing. ***F***, Maximum whole-cell conductance of HCN channels (G_h), calculated from tail currents at −100 mV, increased 13.3-fold between hearing onset and maturity, while the leak conductance (G_{Leak}) exhibited a much smaller change (1.8-fold). Data points binned in 3 d increments ($n = 7$–16 for all bins). Sigmoidal fit (G_h): half-maximal age, P16.5 ± 0.3, slope 2.2 ± 0.3 d. Slope of linear fit (G_{Leak}): 0.3 nS/d. ***G***, Analyses of tail currents of MSO neurons of three different ages (P9, P14, and P21) show strong differences in the voltage sensitivity of activation [half-maximal activation voltage of Boltzmann fits indicated by dotted lines; voltage steps between −30 mV and either −110 mV (P14, 21) or −120 mV (P9)]. ***H***, Group data showing the time course of a 30 mV depolarizing shift in $V_{1/2}$. Boltzmann fit to the data show that the shift is 50% complete at P15 (dotted line). At the average resting potential of −58 mV in electrophysiologically mature (>P18) MSO neurons, nearly half of I_h is activated. Ctl, Control; PND, postnatal day.

k is the slope factor. The whole-cell capacitance varied from 18.1 ± 1.4 pF (≤P11) to 20.7 ± 0.9 pF (≥P18), and was obtained from the capacitance neutralization circuitry of the amplifier. This increase likely reflects the slight increase in somatic membrane surface area shown by quantitative anatomical analyses (Rautenberger et al., 2009).

In all experiments, values are presented as mean ± SEM, and statistical significance was assessed using either a two-way ANOVA or Student's *t* test at a significance level (α) of 0.05.

Immunofluorescence labeling

Animals were anesthetized with xylazine (20 mg/kg) and ketamine (150 mg/kg), and were killed by intracardiac perfusion with cold PBS, followed by 4% paraformaldehyde. Brains were removed and postfixed overnight in 4% paraformaldehyde and transferred to a 30% sucrose solution overnight. Tissues were placed in ornithine carbamyl transferase embedding medium (Tissue Tek) and frozen by immersion in a dry ice-chilled isopentane bath. Thirty-micrometer horizontal sections were cut using a cryostat and were processed for immunofluorescence labeling. The slices were first fixed in 4% paraformaldehyde in PBS for 10 min, then sections were incubated in blocking buffer (0.3% Triton X-100 mixed with 5% goat serum in PBS) for 30 min at room temperature, followed by an overnight incubation with primary antibody in blocking buffer (4°C). Sections were then washed in PBS for 3 × 10 min and incubated in Alexa Fluor 405-, 488-, or 555-conjugated secondary antibodies for 2 h. After washing, slices were mounted on superfrost/plus slides with PermaFluor mounting reagent (Thermo Scientific). The following antibodies were used in this study: guinea pig polyclonal anti-HCN1 (Shin and Chetkovich, 2007) and anti-HCN2 (Shin et al., 2006), 1:1000; mouse monoclonal anti-HCN4 (N114/10), 1:500 [University of California (UC) Davis/NIH NeuroMab Facility, Davis, CA]; and rabbit monoclonal anti-synaptophysin (SYN) antibodies, 1:500 (Millipore). The adult pattern of HCN1, HCN2, and HCN4 labeling in gerbil hippocampus (and thalamus for HCN4) was similar to that of mice (data not shown). HCN3 subunit expression was not pursued because commercial antibodies [Millipore Bioscience Research Reagents (MAB5598), Neuromab (75–175), and Alomone Labs (APC-057)] do not specifically recognize HCN3 in gerbil tissue.

Fluorescence microscopy

Low-power images were obtained on a TissueGnostics imaging system. Briefly, for specifying the imaging area, the slide was previewed with an EC Plan-Neofluar 2.5× objective [numerical aperture (NA) 0.075] under a single channel. Then imaging parameters were setup (fixed *x* and *y* speed, acceleration, automatic focusing range in *z*-axis, scanning mode, exposure time, and digital offset). Then higher-power images were acquired through an EC Plan-Neofluar 20× objective (NA 0.5).

Confocal microscopy and image analysis

Images were obtained on a Zeiss LSM 510 META laser scanning confocal (Plan-Apochromat 63× objective/1.4 NA oil Ph3). For experiments on sections costained with different combinations of antibodies with anti-synaptophysin, images were taken using fixed confocal settings (Scaling: *x*, 0.056 μm; *y*, 0.056 μm; *z*, 1 μm; image size, 512 × 512 pixels; 8-bit; zoom, 3; pixel dwell, 2.51 μs; average, line 8; master gain, 650; digital gain, 1; digital offset, −0.15; lasers: 6% for 405 nm, 8% for 488 nm, 15%

for 543 nm; pinholes: 78 μm for Ch-405, 86 μm for Ch-488 nm, and 96 μm for Ch-543 nm. All confocal images were obtained from the same range of section depth (the stack containing 10 slices was taken from a 9 μm range by 1 μm intervals at the center of a 30-μm-thick section). For image analysis, several custom macros were independently run with NIH ImageJ software to automatically carry out background correction and thresholding for different slices.

Western blots

Tissue preparation and Western blotting were performed as previously described (Lewis et al., 2009) with some modifications. Briefly, the MSO tissues of four to five pre-hearing (P7–P11) or mature (P18–P24) animals were homogenized immediately after subdissection in buffer containing 50 mM Tris-HCl, pH 7.4, 150 mM NaCl, 1% Nonidet-40, 0.1% SDS, 0.5% sodium desoxycholate, 5 mM EDTA, and a mixture of protease inhibitors (Roche). The homogenates were centrifuged at 20,000 × *g* at 4°C for 10 min, and the supernatant was collected and frozen until further use. Protein concentrations were determined with the Bradford protein assay (Bio-Rad). For Western blotting, extracts were mixed with sample buffer, boiled at 95°C for 5 min, cooled on ice for 2 min, and separated on 10% SDS-PAGE at 150 V under denaturing conditions. Proteins were blotted on PVDF membranes, and the blots were blocked in 5% milk in TBST solution for 30 min, and incubated with primary antibodies at 4°C overnight. Then the blots were rinsed in TBST for 3 × 10 min and incubated in HRP-conjugated secondary antibody for 1 h. Antibody binding was detected using SuperSignal West Pico Chemiluminescent Substrate (Thermo Scientific), and quantified by densitometry from blots with linear signal using NIH ImageJ software. α-Tubulin expression was used for loading control. The relative subunit proportions were calculated by dividing the α-tubulin normalized mature density by that of pre-hearing. For the present study, the following antibodies and dilutions were used for Western blotting: guinea pig anti-HCN1 (Shin and Chetkovich, 2007), 1:2000; guinea pig anti-HCN2 (Shin et al., 2006), 1:2000; mouse anti-HCN4 (N114/10, UC Davis/NIH NeuroMab Facility), 1:1000; and mouse anti-α-tubulin (DM1A, Santa Cruz Biotechnology), 1:5000. Normalized data were analyzed using unpaired, two-tailed Student's *t* test, with significance considered as $p < 0.05$.

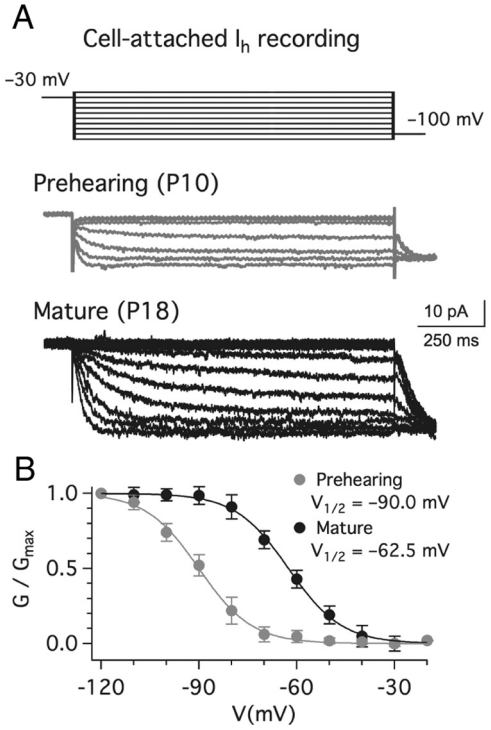

Figure 2. Noninvasive measurements of the voltage dependence of I_h activation. ***A***, Cell-attached patch recordings from a P10 and P18 MSO principal neuron. Top, Voltage protocol (10 mV step increment); bottom, current responses. ***B***, Group data: normalized conductance plot from cell-attached patch recordings. Solid lines are Boltzmann fits to the average data. The $V_{1/2}$ for pre-hearing (P10–P12) and mature ages (P18–P22): −90.0 ± 0.5 and −62.5 ± 0.3 mV, respectively; k = −8.2 ± 0.3 and −8.1 ± 0.4, respectively. The $V_{1/2}$ and k values in cell-attached recordings were statistically indistinguishable from those in whole-cell recordings ($p > 0.5$, $n = 7$ for conditions).

Results

To examine the functional impact of I_h around the onset of hearing (~P12 in gerbils), we made whole-cell current-clamp recordings in brainstem slices from gerbils, a rodent exhibiting prominent low-frequency hearing similar to humans. During development, I_h played an increasingly important role in setting the resting membrane properties of MSO principal neurons (Fig. 1). Blockade of I_h with 50 μM ZD7288 increased the input resistance 1.8-fold before hearing (P9–P11), and 5.4-fold after 1 week of auditory experience (Fig. 1*B*; P21–P23; $p < 0.05$; n = 5–10 per bin). I_h blockade hyperpolarized the resting potential by 9 mV before hearing onset, and 13 mV during the first week of hearing (Fig. 1*C*). Analyses of pharmacologically isolated I_h in whole-cell voltage-clamp experiments revealed that over the first week of hearing between P12 and P19, I_h increased progressively in magnitude, up to ~13-fold (average maximal conductance: P6–P8, 5.28 ± 0.0.62 nS; P30–P32, 70.17 ± 0.7.22 nS), while in the same neurons passive leak current was relatively stable over development (Fig. 1*D*,*F*). Together with the increase in magnitude, I_h exhibited progressively faster activation and deactivation kinetics with development (Fig. 1*E*). Currents at both ages exhibited dual exponential time constants of activation, τ_{fast} and τ_{slow} (pre-hearing: τ_{fast} 96.5 ± 12.3 ms, τ_{slow} 1.0 ± 0.2 s, n = 15; mature: τ_{fast} 26.3 ± 2.1 ms, τ_{slow} 0.19 ± 0.02 s, n = 22). Most surprisingly, analyses of tail currents revealed that the half-activation voltage of I_h ($V_{1/2}$) shifted nearly 30 mV in the depolarizing direction during the first week of hearing, from −90 to −61 mV (Fig. 1*G*,*H*). Although whole-cell dialysis of the intracellular contents of cells induced a progressive shift in both the maximal conductance and $V_{1/2}$ of I_h, particularly with larger pipette sizes (up to 20% decrease in maximal conductance and 6 mV negative shift in $V_{1/2}$ for recordings with pipettes of 2–3 MΩ open tip resistance), we reduced these effects to acceptable levels by confining patch pipettes to smaller sizes. The average change in maximal conductance and $V_{1/2}$ was <10% and −2 mV over the first 30 min of recording with pipettes having 5–8 MΩ open-tip resistance. Measurements of $V_{1/2}$ in cell-attached patch recordings, in the absence of perturbations of the intracellular environment, agreed well with those from whole-cell recordings (cell-attached vs whole-cell measurements: $V_{1/2}$ = −90 vs −90 mV at pre-hearing ages; −63 vs −61 mV at mature ages) (Fig. 2).

The increasing block of input conductance by ZD7288 after hearing onset suggested that HCN channel expression was increased in older animals. We thus performed Western blotting of subdissected gerbil MSO tissue. Consistent with developmental increases in I_h, we found dramatic increases in HCN1, HCN2, and HCN4 subunit expression in animals >P21 ("mature") compared with P9 ("pre-hearing") (Fig. 3). Changes in I_h properties in electrophysiologically mature MSO neurons could occur either through alterations of the subunit composition of HCN channels or through their modulation. To evaluate subunit composition, we examined the immunofluorescence expression of HCN subunits in MSO principal neurons over development (Fig. 4). Dual immunofluorescence labeling for synaptophysin and HCN subunits (see Materials and Methods) showed that at P9, HCN1 immunoreactivity was diffuse and extensively cytoplasmic in MSO principal neurons, whereas at ages >P21, HCN1 labeling

was intense and appeared enriched at the plasma membrane (Fig. 4*A*,*B*,*G*,*H*), consistent with a previous immunolabeling study (Koch et al., 2004). HCN2 immunoreactivity was weak before hearing onset, and increased dramatically at ages >P21, similar to HCN1. However, in contrast to HCN1 staining, almost all HCN2 immunoreactivity was restricted to neuropil unassociated with either presynaptic or postsynaptic labeling of MSO principal neurons (Fig. 4*C*,*D*,*I*,*J*). Many small cell bodies were also HCN2 positive (Fig. 4*I*,*J*, small asterisks), possibly corresponding to an HCN2-positive subpopulation of oligodendrocytes previously reported (Notomi and Shigemoto, 2004). HCN4 expression most closely resembled that of HCN1, with minimal staining of membranes in MSO principal neurons at P9 and striking membrane enrichment at ages >P21 (Fig. 4*E*,*F*,*K*,*L*). Although low expression levels at P9 precluded resolution of the HCN subunit complement of pre-hearing gerbils, immunofluorescence labeling is consistent with the electrophysiological results of Figure 1, showing strong upregulation of I_h during the first week of hearing, and identifies HCN1 and HCN4, but not HCN2, as the primary underlying subunits.

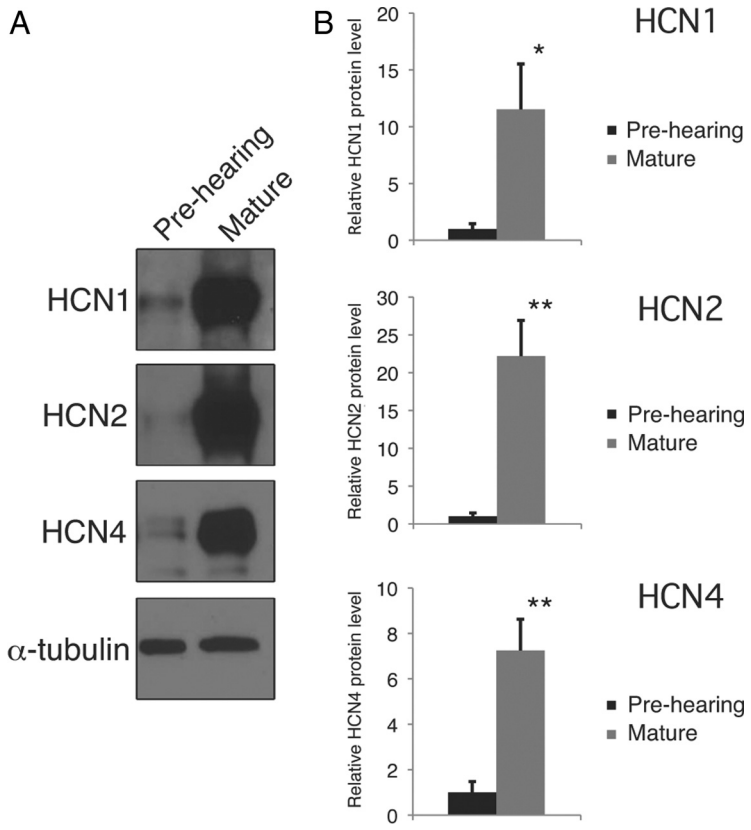

Figure 3. Western blots of gerbil MSO. ***A***, Western blotting was performed with lysates derived from subdissected gerbil MSO at pre-hearing or mature ages using antibodies against HCN1, HCN2, HCN4, or α-tubulin. Five gerbils of each age were used for HCN1 and HCN2 blots, four gerbils of each age were used for HCN4 blots. *$p < 0.05$, **$p < 0.01$, unpaired, two-tailed *t* test. The pre-hearing animals were 7–11 d old, and mature animals were 18–24 d old. ***B***, Relative level of HCN protein in mature versus pre-hearing ages.

To explore whether modulation of HCN channels by intracellular second messengers might also contribute to developmental changes in I_h in the MSO, we compared I_h recorded in whole cells versus nucleated patches (Fig. 5). If changes in subunit composition alone underlie the maturation of biophysical properties of I_h, then I_h in whole-cell and nucleated patches should exhibit similar kinetics and voltage dependence. In contrast, because the cytoplasm undergoes rapid dialysis in nucleated patches, differences between whole-cell and nucleated patches would be predicted if developmental differences in I_h biophysical properties were dependent upon modulation by intracellular second messengers or signaling events such as phosphorylation. Surprisingly, we found that in nucleated patches from animals at ages >P18, rather than the mature biophysical properties observed in the whole-cell configuration, both the kinetics and voltage sensitivity of I_h activation were statistically indistinguishable from I_h recorded in whole cells before the onset of hearing (pre-hearing: P6–P12) (Fig. 5*A*–*C*). The $V_{1/2}$ of activation shifted negatively to −90 mV, while both the fast (τ_{fast}) and slow activation time (τ_{slow}) constants were increased (slowed) by factors of 4 and 7, respectively (for steps from −30 to −90 mV: $\tau_{fast} = 122.5 \pm 25.8$ ms; $\tau_{slow} = 1487 \pm 403$ ms) (Fig. 5*C*, left and center graphs). The relative proportion of the fast kinetic component of I_h increased progressively from 0.38 ± 0.06 to 0.74 ± 0.01 between pre-hearing and mature ages ($n = 22$ and 15, respectively; $p < 0.01$). However, the relative proportion of the fast component of I_h in dialyzed nucleated patches was not significantly different from the value obtained from pre-hearing whole-cell recordings (0.39 ± 0.05, $n = 11$) (Fig. 5*C*, right graph). These results indicate that modulation via diffusible substances plays a critical role in producing the large developmental shift in the biophysical properties of I_h. We next examined the developmental role of three modulators known to affect I_h: cAMP, p38 MAP kinase, and PIP_2 (Fig. 5*D*–*F*). In whole-cell recordings, antagonists of p38 MAP kinase and PIP_2 signaling (SB203580 and wortmannin, respectively) produced negative shifts in the activation range of I_h. These shifts increased during development: blockade of p38 MAP kinase with bath application of 10 μM SB203580 hyperpolarized the activation $V_{1/2}$ by 4 mV before hearing at P10, but 11 mV at P18 (shift at P18 was significantly different from P10, $p < 0.05$). Likewise, inhibition of PIP_2 signaling with 20 μM wortmannin produced a 2 mV hyperpolarizing shift in $V_{1/2}$ at P10, but 8 mV at P18 ($p < 0.05$; Fig. 5*D*). These results were not significantly affected by whole-cell dialysis, as shifts in activation were the same when slices were preincubated with modulators >45 min before recordings and measurements of activation were made immediately after break-in (data not shown). Measurements were made in the presence of either a P38 MAP kinase antagonist (10 μM SB203580 or 10 μM SB202190, $n = 8$ and 4, respectively), or 20 μM wortmannin ($n = 7$; $p > 0.5$ for comparisons of activation $V_{1/2}$ and k for acute application vs preincubation experiments). By contrast, activation of cAMP with 300 μM dB-cAMP or 100 μM forskolin produced large depolarizing shifts in $V_{1/2}$ before hearing at P10, but the size of the shift progressively declined over the subsequent week, with no significant change in $V_{1/2}$ detected at P18 ($p = 0.78$) (Fig. 5*E*), indicating either that I_h becomes insensitive to cAMP modulation by P18 or that the modulatory effect of cAMP has reached saturation.

To test whether I_h in nucleated patches from older animals retains the capability of being modulated, we pulled nucleated patches in the presence of two endogenous neuromodulators of I_h in the pipette solution (Fig. 5*F*). Addition of 300 μM dB-cAMP or 100 μM PIP_2 shifted the $V_{1/2}$ of activation by 10.8 and 12.4 mV,

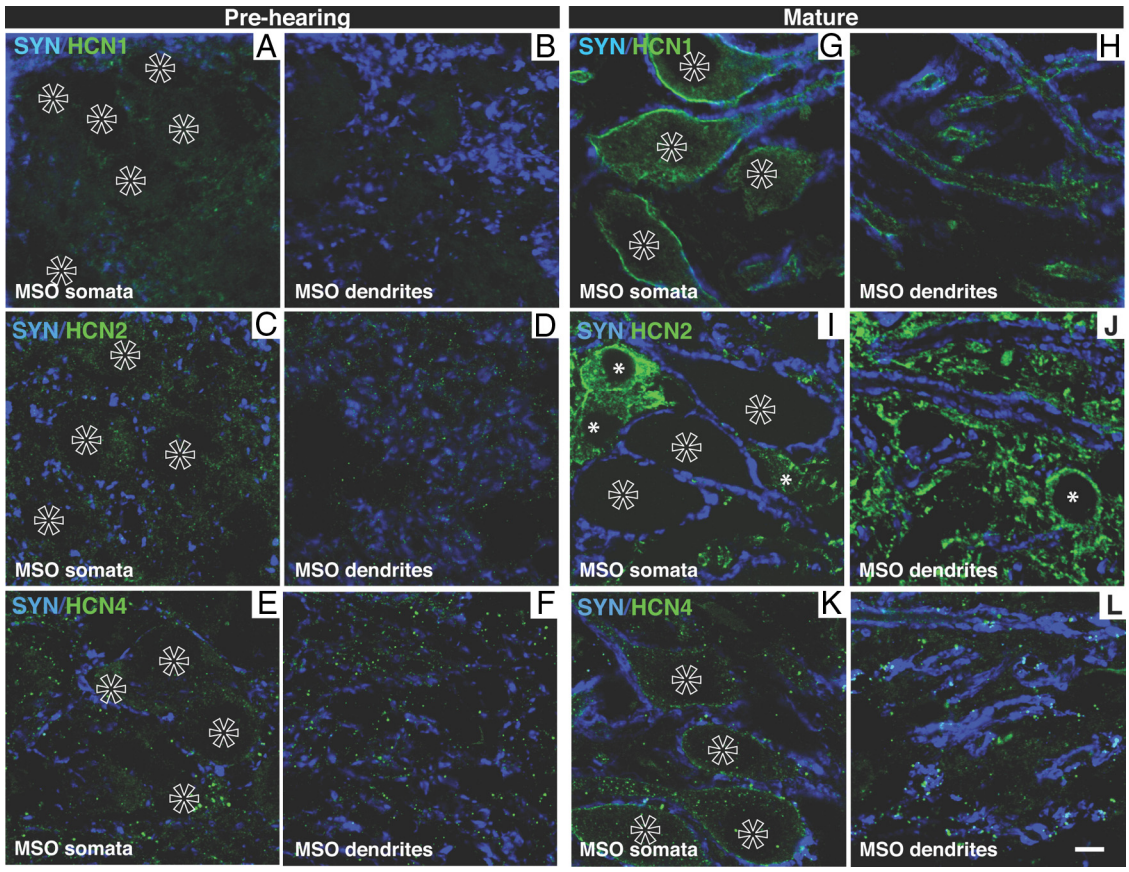

Figure 4. Distinct HCN1 and HCN2 distribution in juvenile and adult gerbil MSO. ***A–F***, Before the onset of hearing (P9), scattered synaptophysin-positive presynaptic terminals (SYN; blue) and low levels of HCN1 (***A***, ***B***, green) and HCN2 (***C***, ***D***, green), and HCN4 (***E***, ***F***, green) expression were observed in the somata of principal neurons (***A***, ***C***, ***E***, open asterisks) and dendrites (***B***, ***D***, ***F***). ***G–L***, In contrast, ~1 week after onset of discriminatory hearing (P22), distinct patterns of HCN1, HCN2, and HCN4 expression were observed in MSO neurons. Specifically, along with diffuse staining of the cytoplasm, HCN1 immunoreactivity (***G***, ***H***, green) was enriched at the membrane of both somata (***G***, open asterisks) and dendrites (***H***), often juxtaposing SYN-positive presynaptic terminals (blue). Interestingly, HCN2 immunoreactivity was not observed in somata or dendrites of principal neurons, but was present in smaller cells (solid asterisks) and neuropil in the MSO (***I***, ***J***). HCN4 immunoreactivity was observed in both the soma and dendrites but at lower levels than that for HCN1 (***K***, ***L***). Scale bar, 5 μm.

respectively (-77.8 ± 1.1 and -76.2 ± 2.3 mV vs control: -88.6 ± 0.7 mV, $p < 0.01$). The effects of dB-cAMP and PIP_2 were additive, shifting the $V_{1/2}$ of activation by 21.3 mV (-67.3 ± 4.3 mV vs control: -88.6 ± 0.7 mV, $p < 0.01$). These findings have two implications. First, the apparent progressive decrease in the modulatory effects of cAMP agonists after hearing onset is likely due to the saturation of naturally occurring cAMP modulation before extrinsic cAMP application. Second, the agonist-induced restoration of both cAMP and PIP_2 modulation in nucleated patches supports the conclusion that the striking similarity of I_h properties in nucleated patches to I_h before the onset of hearing is primarily due to the loss of diffusible modulatory factors.

We conclude that developmentally regulated neuromodulation of I_h shifts the underlying channels' voltage sensitivity into the physiological voltage range near rest (approximately −58 mV). This shift combined with the 13-fold developmental increase in conductance allow I_h to play an increasingly important role in setting a high resting conductance that in turn speeds voltage changes and increases the temporal resolution of MSO principal neurons. To test this functional role, we compared the time resolution of synaptic coincidence detection of bilateral excitatory inputs in normal ACSF with conditions under which I_h was either blocked or modulated (Fig. 6; see Materials and Methods). Under control conditions, the probability of firing an action potential was 0.5 ($p_{0.5}$) when the ITD was 194 μs (Fig. 6*A*,*B*, black circles). However, the $p_{0.5}$ increased in duration by ~300% when I_h was blocked with ZD7288 applied either externally at 50 μM (purple squares, $p_{0.5} = 563$ μs) or internally through its inclusion in the patch pipette (20 μM; open diamonds, $p_{0.5} = 557$ μs). Although externally applied ZD7288 is known to affect synaptic transmission, the identical results obtained with internal ZD7288 preclude the possibility that these nonspecific effects of the drug significantly alter the width of the ITD function. When the hyperpolarized resting potential was restored to control levels with current injection through the patch pipette, the $p_{0.5}$ decreased to 374 μs (Fig. 6*A*,*B*, blue traces and triangles), indicating that I_h mediates an increase in temporal resolution directly through its contribution to the cell's resting conductance as well as indirectly, presumably because the depolarization of the resting potential activated low-voltage-activated potassium channels. Finally, when the activation range of I_h was shifted negatively by ~10 mV via bath application of the p38 MAP kinase antagonist 10 μM SB203580 (as in Fig. 5*D*), functional I_h was reduced at rest, and hyperpolarized the resting potential by 10 mV (Fig. 6*C*). Under this condition, the resolution of coincidence detection was similar to that when I_h was fully blocked with 50 μM ZD7288, even when drug-induced changes in resting potential were offset with current injection through the pipette ($p_{0.5}$: 331 μs in SB203580 vs 378 μs in SB203580 + ZD7288). These results underscore the high sensitivity of the resolution of binaural coincidence detection to the modulatory state of I_h.

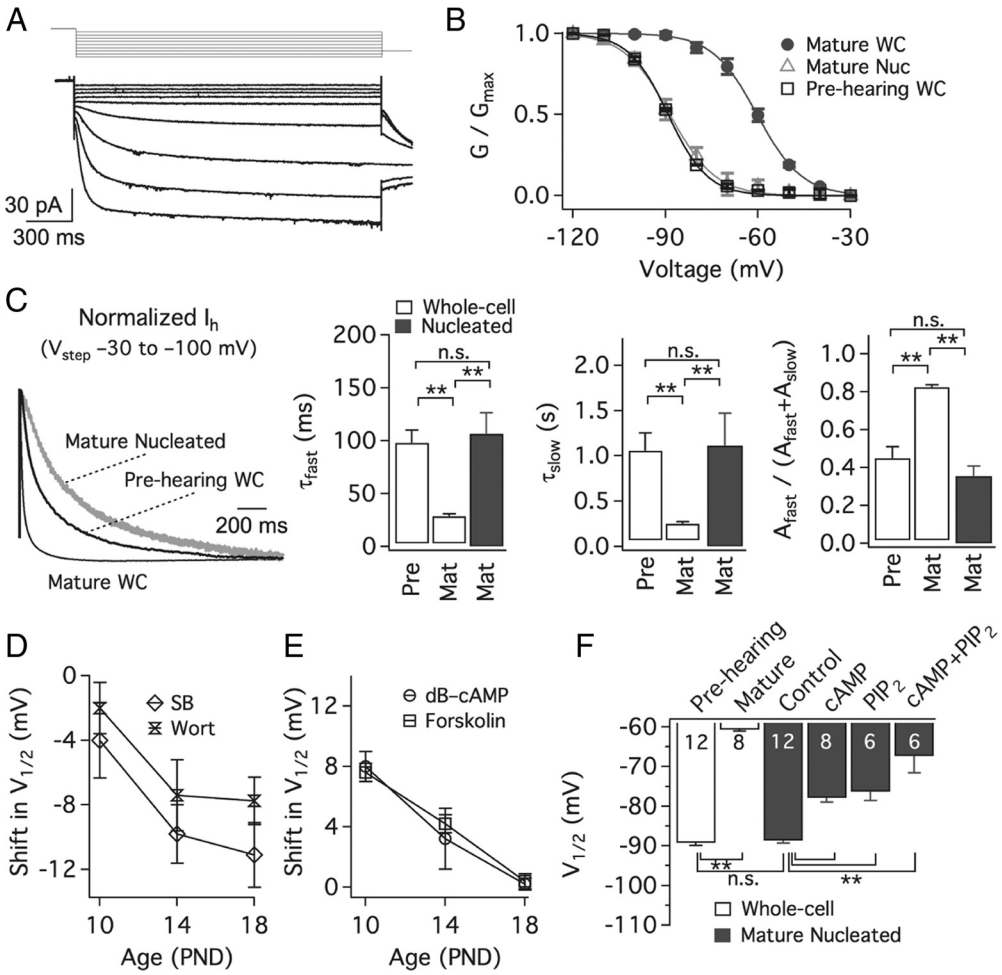

Figure 5. The developmental changes in MSO I_h are largely driven by modulation. ***A***, I_h recorded in nucleated patches from electrophysiologically mature MSO neurons. Voltage protocol: −30 mV (0.5–1 s duration) to voltages between −30 and −120 mV (1 s) in −10 mV steps, followed by a step to −100 mV. ***B***, Normalized conductance of HCN channel (G_h) activation curves in nucleated patches at electrophysiologically mature ages (>P18) are indistinguishable from those obtained in whole-cell recordings from pre-hearing animals (P6–P12). Fits: mature whole-cell, $V_{1/2} = -60$ mV, $k = 7.5$; mature nucleated patches, $V_{1/2} = -89$ mV, $k = 7.4$ mV; pre-hearing whole-cell, $V_{1/2} = -90$ mV, k = 6.5 mV. Whole-cell activation curve from mature ages is included for comparison. Activation $V_{1/2}$ is similar between nucleated patches from mature gerbils and whole-cell recordings from pre-hearing gerbils. ***C***, The activation kinetics and relative proportion of fast and slow kinetics of I_h (at −100 mV) in nucleated patches mimics those of pre-hearing MSO neurons. $^{**}p < 0.01$; n.s., $p > 0.05$ (for *B* and *C*: $n = 22$, 15, and 11, respectively, for WC mature, WC pre-hearing, and nucleated mature). ***D***, Antagonists of PIP_2 signaling (20 μM wortmannin) and P38 MAP kinase (10 μM SB203580) induce larger hyperpolarizing shifts in activation $V_{1/2}$ during early hearing, suggesting an upregulation of the two pathways with age ($n > 6$ for each point). ***E***, Bath application of cAMP agonists (300 μM dB-cAMP and 100 μM forskolin) result in decreasing depolarizing shift, suggesting either a change in cAMP sensitivity or saturation of cAMP signaling with maturation ($n > 5$ for each point). ***F***, Summary of half-activation voltages in whole-cell recordings and nucleated patches (open and gray bars, respectively). Significance levels as in ***C***, and $n > 6$ for all points. Mat, Mature; Pre, pre-hearing; Nuc, nucleated; Wort, wortmannin; PND, postnatal day.

Discussion

To accurately represent the external world during development, neurons in sensory circuits must establish not only the appropriate strength and pattern of synaptic connections, but they must also coordinate synaptic changes with adjustments in intrinsic voltage-gated ion channels. The binaural neurons of the MSO provide a clear-cut example of the need for such coordination, as the interaction between binaural synaptic activity and voltage-gated ion channels allow these neurons to compute information about azimuthal sound location with precise, microsecond resolution. Here we have shown that in MSO principal neurons, modulation of I_h during the first week of hearing causes a 30 mV depolarizing shift in the activation range of the channel. In combination with a concurrent 13-fold increase in maximal conductance, modulation establishes I_h as a powerful resting conductance, conferring membrane properties appropriate for processing interaural time differences with a resolution of tens of microseconds (Goldberg and Brown, 1969; Yin and Chan, 1990; Brand et al., 2002).

Molecular composition of I_h in MSO neurons

The developmental shift of I_h activation in MSO neurons toward more depolarized voltages and faster kinetics likely reflects a progressively greater role of HCN1 subunits, which have been detected immunocytochemically in mature MSO neurons here and in prior studies (Koch et al., 2004; Leao et al., 2006). In expression systems, homomeric HCN1-containing channels exhibit similar fast kinetics on the order of tens of milliseconds (Santoro et al., 2000; Chen et al., 2001; Ulens and Tytgat, 2001). The slower activation time constant we observed in MSO I_h is consistent with the expression of HCN4 in MSO, which exhibits the slowest kinetics of the HCN subunits (Santoro et al., 2000). Interestingly, while HCN1 and HCN4 subunits were robustly expressed in MSO neurons, HCN2 subunits were restricted to the neuropil, reflecting expression in axons as well as in a subset of oligodendrocytes (Notomi and Shigemoto, 2004).

Developmental changes in I_h properties and neuron excitability are typically thought to include alterations in subunit composition (Vasilyev and Barish, 2002; Surges et al., 2006; Brewster et

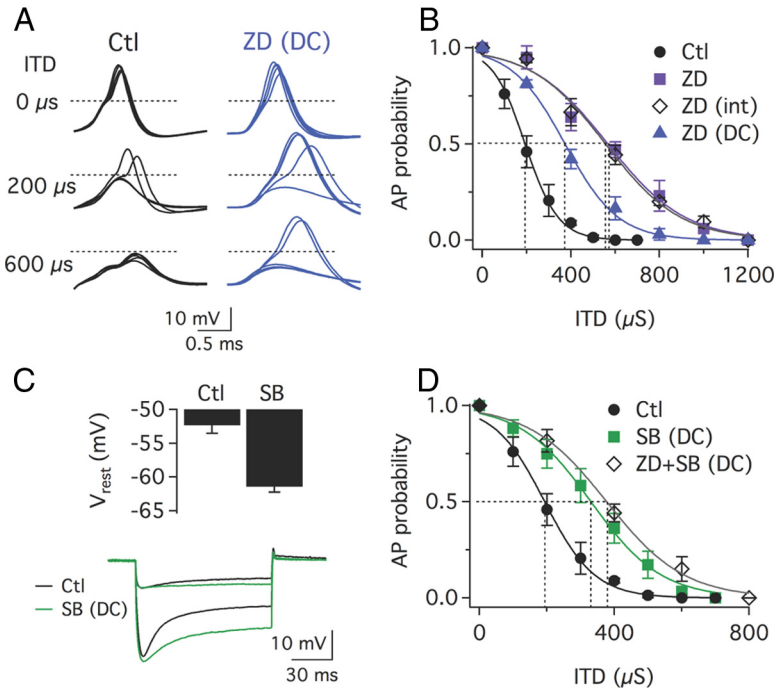

Figure 6. Control of the synaptic coincidence detection by I_h modulation. ***A***, Bilateral excitatory stimulation aligned in time for 100% probability of spike initiation (0 μs ITD), and then offset by 200 or 600 μs [control (Ctl), black traces]. In 50 μM ZD7288, spike probability increased for nonzero ITDs even when the hyperpolarized V_{rest} was restored to control values with constant current [ZD (DC)]. ***B***, The synaptic coincidence window in normal saline (Ctl, circles), 50 μM external ZD7288 either alone (ZD, squares) or with V_{rest} restored with direct current injection [ZD (DC), triangles], or 20 μM internal ZD7288 [ZD (int), diamonds] ($n > 5$ for all cases). Boltzmann fits to the points exhibited half-decay times of 194, 563, 557, and 374 μs for Ctl, ZD, ZD (int), and ZD (DC) conditions. ***C***, Block of P38 MAP kinase by 20 μM SB203580 hyperpolarized the V_{rest} by 10 mV and reduced the delayed depolarizing sag during comparable voltage responses to hyperpolarizing current. ***D***, The synaptic coincidence window was similarly broadened when P38 MAP kinase signaling was antagonized with 10 μM SB203580 alone or after I_h blockade by 50 μM ZD7288 (ZD + SB) ($n > 5$ for all cases). Comparable membrane potentials were maintained in all pharmacological conditions with constant current injection (DC). Curves indicate Boltzmann fits. Half-decay times: 194, 331, and 378 μs, respectively, for Ctl, SB, and SB/ZD conditions.

al., 2007; Hassfurth et al., 2009; Kanyshkova et al., 2009). By contrast, several lines of evidence support a dominant role for intracellular modulation in MSO I_h. First, the ratio of amplitudes of the fast and slow kinetic components of I_h were stable over development, suggesting that the underlying ratio of channel subunits (possibly HCN1 and 4) is consistent even in the face of a 13-fold increase in maximal conductance. Second, when the intracellular environment of HCN channels was extensively dialyzed in nucleated patches from electrophysiologically mature neurons we observed that both the voltage sensitivity and kinetics of I_h were nearly identical to I_h before hearing onset. Although we cannot rule out subtle changes in subunit composition or heteromerization of the expressed subunits, the similarity in I_h before hearing and in mature, dialyzed neurons suggests that the subunit composition of MSO I_h is not the major factor driving functional changes in I_h during development soon after the onset of hearing.

Convergence of multiple I_h modulatory pathways in MSO principal neurons

Before hearing onset, the activation range of I_h in MSO neurons can be shifted positively by 8 mV by cAMP analogs, but this sensitivity is progressively lost during the first week of hearing (Fig. 5*E*). However, cAMP sensitivity was fully restored in excised patches from electrophysiologically mature neurons, where the native modulatory environment had been largely eliminated. Together, these results indicate that the apparent loss of sensitivity to cAMP during development in fact reflects a saturation of cAMP modulation, possibly due to an upregulation in the intracellular level of cAMP itself (Surges et al., 2006) or to changes in the affinity of cAMP for the channel. Given that HCN1 subunits display the least sensitivity to cAMP (Chen et al., 2001; Wainger et al., 2001), the strong cAMP sensitivity in MSO neurons likely results from HCN4 subunits (Seifert et al., 1999; Viscomi et al., 2001; Altomare et al., 2003), which were detected by immunofluorescent staining in both the soma and dendrites of MSO neurons as well as in Western blots of subdissected MSO tissues. We were not able to assess the role of HCN3 subunits due to the lack of specificity of commercial antibodies. However, the shift of the voltage dependence of activation of HCN3 by cAMP is toward more hyperpolarized potentials (Mistrík et al., 2005). It thus seems unlikely that HCN3 plays a significant role in the positive shifts in voltage dependence of MSO I_h during development.

Modulation through cAMP accounts for only approximately a third of the developmental shift in the voltage dependence of I_h activation in MSO neurons. Inhibition of both PIP_2 and p38 MAP kinase showed that these modulatory pathways together can account for nearly an additional 20 mV of the depolarizing developmental shift in activation range. The effects of p38 MAP kinase are consistent with the depolarizing shifts induced by this pathway on I_h in hippocampal CA1 pyramidal neurons (Poolos et al., 2006). PIP_2 has been shown to be a potent modulator of I_h in both neurons and cardiac tissues (Pian et al., 2006; Zolles et al., 2006). Together, cAMP, PIP_2, and p38 MAP kinase can account for about 30 mV of the depolarizing shift during development. However, it is likely that other modulatory mechanisms influence the function of I_h in MSO principal neurons that we have not yet identified. For example, tyrosine kinases that are known to positively shift the voltage dependence of HCN channel activation (Yu et al., 2004; Zong et al., 2005). Possible contributions from other mechanisms do not alter the conclusion that diffusible modulators are the dominant mechanism of developmental changes in I_h in MSO neurons.

Functional impact of I_h modulation for temporal coding

In the mammalian auditory system, I_h and low-voltage-activated potassium channels are typically coexpressed in neurons that encode temporal information (Mo and Davis, 1997; Bal and Oertel, 2000; Koch and Grothe, 2003; Leao et al., 2006; Cao et al., 2007; Hassfurth et al., 2009). A depolarizing shift in I_h activation range could have complex consequences, with the excitatory effect of depolarization toward action potential threshold offset by increased membrane shunting as well as activation of low-voltage-activated potassium channels (Banks et al., 1993; Rothman and Manis, 2003). In MSO principal neurons, I_h modulation clearly results in increased temporal precision. Given the ~50% activation of channels at rest, I_h mediates an enormous resting conduc-

tance that reduces the membrane time constant as well as the window for coincidence detection by ~300%, and the strong 13 mV depolarization of the resting potential effectively recruits low-voltage-activated potassium channels that are known to strongly sharpen binaural coincidence detection (Reyes et al., 1996; Svirskis et al., 2002, 2004; Scott et al., 2005; Mathews et al., 2010).

Interestingly, while principal cells of the avian MSO (nucleus laminaris) exhibit a high density of HCN channels, activation occurs at more negative potentials ($V_{1/2} = -86$ mV) (Yamada et al., 2005), thus contributing a smaller resting conductance (Kuba et al., 2005). While the unusually strong role of I_h modulation described in the present study appears to have evolved as a feature of mammalian auditory circuits, it is important to note that, unlike MSO principal cells, neurons in nucleus laminaris receive depolarizing GABAergic inhibition both tonically and phasically, which sharpens binaural coincidence detection both through a shunting mechanism (Hyson et al., 1995; Funabiki et al., 1998; Yang et al., 1999; Tang et al., 2011) as well as through the activation of low-voltage-gated potassium channels (Howard et al., 2007). Thus, it appears that some of the critical functional roles served by I_h in the mammalian MSO are performed by GABAergic inhibition in birds.

The striking changes in I_h channel density and activation range were closely correlated with the onset of hearing near P12 and were largely complete after 1 week of auditory experience. The first week of hearing is a particularly dynamic period for the development of brainstem auditory pathways and binaural hearing (Rubel and Fritzsch, 2002; Kandler and Gillespie, 2005). Low-voltage-activated potassium currents, known to impart fast integrative properties to MSO principal cells (Svirskis et al., 2002; Mathews et al., 2010), increase by 400% over this time (Scott et al., 2005) and likely mediate much of the I_h-insensitive developmental change in input resistance observed in the present study (Fig. 1*B*). At the same time, glycinergic inhibition, an important circuit component for processing interaural time differences (Brand et al., 2002; Pecka et al., 2008; Jercog et al., 2010), becomes progressively restricted to the soma and exhibits more rapid kinetics (Smith et al., 2000; Kapfer et al., 2002; Magnusson et al., 2005). These physiological dynamics occur during a time when the length and branching patterns of the dendrites have largely stabilized (Rogowski and Feng, 1981; Rautenberger et al., 2009). The present results on I_h provide strong evidence that the encoding of sound localization cues through the binaural circuits of the brainstem depends not only on the appropriate refinement of synaptic connections, but also on coordinated changes in voltage-gated ion channels.

References

Altomare C, Terragni B, Brioschi C, Milanesi R, Pagliuca C, Viscomi C, Moroni A, Baruscotti M, DiFrancesco D (2003) Heteromeric HCN1-HCN4 channels: a comparison with native pacemaker channels from the rabbit sinoatrial node. J Physiol 549:347–359.

Bal R, Oertel D (2000) Hyperpolarization-activated, mixed-cation current (I(h)) in octopus cells of the mammalian cochlear nucleus. J Neurophysiol 84:806–817.

Banks MI, Pearce RA, Smith PH (1993) Hyperpolarization-activated cation current (IH) in neurons of the medial nucleus of the trapezoid body: voltage clamp analysis and enhancement by norepinephrine and cAMP suggest a modulatory mechanism in the auditory brainstem. J Neurophysiol 70:1420–1432.

Bellingham MC, Lim R, Walmsley B (1998) Developmental changes in EPSC quantal size and quantal content at a central glutamatergic synapse in rat. J Physiol 511:861–869.

Brand A, Behrend O, Marquardt T, McAlpine D, Grothe B (2002) Precise inhibition is essential for microsecond interaural time difference coding. Nature 417:543–547.

Brenowitz S, Trussell LO (2001) Maturation of synaptic transmission at end-bulb synapses of the cochlear nucleus. J Neurosci 21:9487–9498.

Brewster AL, Chen Y, Bender RA, Yeh A, Shigemoto R, Baram TZ (2007) Quantitative analysis and subcellular distribution of mRNA and protein expression of the hyperpolarization-activated cyclic nucleotide-gated channels throughout development in rat hippocampus. Cereb Cortex 17:702–712.

Cao XJ, Shatadal S, Oertel D (2007) Voltage-sensitive conductances of bushy cells of the mammalian ventral cochlear nucleus. J Neurophysiol 97:3961–3975.

Chen S, Wang J, Siegelbaum SA (2001) Properties of hyperpolarization-activated pacemaker current defined by coassembly of HCN1 and HCN2 subunits and basal modulation by cyclic nucleotide. J Gen Physiol 117:491–504.

Chirila FV, Rowland KC, Thompson JM, Spirou GA (2007) Development of gerbil medial superior olive: integration of temporally delayed excitation and inhibition at physiological temperature. J Physiol 584:167–190.

DiFrancesco D (1993) Pacemaker mechanisms in cardiac tissue. Annu Rev Physiol 55:455–472.

Funabiki K, Koyano K, Ohmori H (1998) The role of GABAergic inputs for coincidence detection in the neurones of nucleus laminaris of the chick. J Physiol 508:851–869.

Goldberg JM, Brown PB (1969) Response of binaural neurons of dog superior olivary complex to dichotic tonal stimuli: some physiological mechanisms of sound localization. J Neurophysiol 32:613–636.

Golding NL, Robertson D, Oertel D (1995) Recordings from slices indicate that octopus cells of the cochlear nucleus detect coincident firing of auditory nerve fibers with temporal precision. J Neurosci 15:3138–3153.

Hassfurth B, Magnusson AK, Grothe B, Koch U (2009) Sensory deprivation regulates the development of the hyperpolarization-activated current in auditory brainstem neurons. Eur J Neurosci 30:1227–1238.

Howard MA, Burger RM, Rubel EW (2007) A developmental switch to GABAergic inhibition dependent on increases in Kv1-type K^+ currents. J Neurosci 27:2112–2123.

Hyson RL, Reyes AD, Rubel EW (1995) A depolarizing inhibitory response to GABA in brainstem auditory neurons of the chick. Brain Res 677:117–126.

Jercog PE, Svirskis G, Kotak VC, Sanes DH, Rinzel J (2010) Asymmetric excitatory synaptic dynamics underlie interaural time difference processing in the auditory system. PLoS Biol 8:e1000406.

Joshi I, Shokralla S, Titis P, Wang LY (2004) The role of AMPA receptor gating in the development of high-fidelity neurotransmission at the calyx of Held synapse. J Neurosci 24:183–196.

Kandler K, Gillespie DC (2005) Developmental refinement of inhibitory sound-localization circuits. Trends Neurosci 28:290–296.

Kanyshkova T, Pawlowski M, Meuth P, Dubé C, Bender RA, Brewster AL, Baumann A, Baram TZ, Pape HC, Budde T (2009) Postnatal expression pattern of HCN channel isoforms in thalamic neurons: relationship to maturation of thalamocortical oscillations. J Neurosci 29:8847–8857.

Kapfer C, Seidl AH, Schweizer H, Grothe B (2002) Experience-dependent refinement of inhibitory inputs to auditory coincidence-detector neurons. Nat Neurosci 5:247–253.

Khurana S, Remme MW, Rinzel J, Golding NL (2011) Dynamic interaction of I_h and $I_{K\text{-}LVA}$ during trains of synaptic potentials in principal neurons of the medial superior olive. J Neurosci 31:8936–8947.

Koch U, Grothe B (2003) Hyperpolarization-activated current (Ih) in the inferior colliculus: distribution and contribution to temporal processing. J Neurophysiol 90:3679–3687.

Koch U, Braun M, Kapfer C, Grothe B (2004) Distribution of HCN1 and HCN2 in rat auditory brainstem nuclei. Eur J Neurosci 20:79–91.

Koike-Tani M, Kanda T, Saitoh N, Yamashita T, Takahashi T (2008) Involvement of AMPA receptor desensitization in short-term synaptic depression at the calyx of Held in developing rats. J Physiol 586:2263–2275.

Kuba H, Yamada R, Fukui I, Ohmori H (2005) Tonotopic Specialization of Auditory Coincidence Detection in Nucleus Laminaris of the Chick. J Neurosci 25:1924–1934.

Leao KE, Leao RN, Sun H, Fyffe RE, Walmsley B (2006) Hyperpolarization-activated currents are differentially expressed in mice brainstem auditory nuclei. J Physiol 576:849–864.

Lewis AS, Schwartz E, Chan CS, Noam Y, Shin M, Wadman WJ, Surmeier DJ,

Baram TZ, Macdonald RL, Chetkovich DM (2009) Alternatively spliced isoforms of TRIP8b differentially control h channel trafficking and function. J Neurosci 29:6250–6265.

Ludwig A, Zong X, Jeglitsch M, Hofmann F, Biel M (1998) A family of hyperpolarization-activated mammalian cation channels. Nature 393:587–591.

Magee JC (1999) Dendritic Ih normalizes temporal summation in hippocampal CA1 neurons. Nat Neurosci 2:848.

Magnusson AK, Kapfer C, Grothe B, Koch U (2005) Maturation of glycinergic inhibition in the gerbil medial superior olive after hearing onset. J Physiol 568:497–512.

Mathews PJ, Jercog PE, Rinzel J, Scott LL, Golding NL (2010) Control of submillisecond synaptic timing in binaural coincidence detectors by K(v)1 channels. Nat Neurosci 13:601–609.

McCormick DA, Pape HC (1990) Properties of a hyperpolarization-activated cation current and its role in rhythmic oscillation in thalamic relay neurones. J Physiol 431:291–318.

Mistrík P, Mader R, Michalakis S, Weidinger M, Pfeifer A, Biel M (2005) The murine HCN3 gene encodes a hyperpolarization-activated cation channel with slow kinetics and unique response to cyclic nucleotides. J Biol Chem 280:27056–27061.

Mo ZL, Davis RL (1997) Heterogeneous voltage dependence of inward rectifier currents in spiral ganglion neurons. J Neurophysiol 78:3019–3027.

Notomi T, Shigemoto R (2004) Immunohistochemical localization of Ih channel subunits, HCN1-4, in the rat brain. J Comp Neurol 471:241–276.

Pecka M, Brand A, Behrend O, Grothe B (2008) Interaural time difference processing in the mammalian medial superior olive: the role of glycinergic inhibition. J Neurosci 28:6914–6925.

Pian P, Bucchi A, Robinson RB, Siegelbaum SA (2006) Regulation of gating and rundown of HCN hyperpolarization-activated channels by exogenous and endogenous PIP2. J Gen Physiol 128:593–604.

Poolos NP, Bullis JB, Roth MK (2006) Modulation of h-channels in hippocampal pyramidal neurons by p38 mitogen-activated protein kinase. J Neurosci 26:7995–8003.

Rautenberger PL, Grothe B, Felmy F (2009) Quantification of the three-dimensional morphology of coincidence detector neurons in the medial superior olive of gerbils during late postnatal development. J Comp Neurol 517:385–396.

Reyes AD, Rubel EW, Spain WJ (1996) In vitro analysis of optimal stimuli for phase-locking and time-delayed modulation of firing in avian nucleus laminaris neurons. J Neurosci 16:993–1007.

Robinson RB, Siegelbaum SA (2003) Hyperpolarization-activated cation currents: from molecules to physiological function. Annu Rev Physiol 65:453–480.

Rogowski BA, Feng AS (1981) Normal postnatal development of medial superior olivary neurons in the albino rat: a Golgi and Nissl study. J Comp Neurol 196:85–97.

Rothman JS, Manis PB (2003) The roles potassium currents play in regulating the electrical activity of ventral cochlear nucleus neurons. J Neurophysiol 89:3097–3113.

Rubel EW, Fritzsch B (2002) Auditory system development: primary auditory neurons and their targets. Annu Rev Neurosci 25:51–101.

Santoro B, Liu DT, Yao H, Bartsch D, Kandel ER, Siegelbaum SA, Tibbs GR (1998) Identification of a gene encoding a hyperpolarization-activated pacemaker channel of brain. Cell 93:717–729.

Santoro B, Chen S, Luthi A, Pavlidis P, Shumyatsky GP, Tibbs GR, Siegelbaum SA (2000) Molecular and functional heterogeneity of hyperpolarization-activated pacemaker channels in the mouse CNS. J Neurosci 20:5264–5275.

Sather W, Dieudonné S, MacDonald JF, Ascher P (1992) Activation and desensitization of N-methyl-D-aspartate receptors in nucleated outside-out patches from mouse neurones. J Physiol 450:643–672.

Scott LL, Mathews PJ, Golding NL (2005) Posthearing developmental refinement of temporal processing in principal neurons of the medial superior olive. J Neurosci 25:7887–7895.

Scott LL, Mathews PJ, Golding NL (2010) Perisomatic voltage-gated sodium channels actively maintain linear synaptic integration in principal neurons of the medial superior olive. J Neurosci 30:2039–2050.

Seifert R, Scholten A, Gauss R, Mincheva A, Lichter P, Kaupp UB (1999) Molecular characterization of a slowly gating human hyperpolarization-activated channel predominantly expressed in thalamus, heart, and testis. Proc Natl Acad Sci U S A 96:9391–9396.

Shin M, Chetkovich DM (2007) Activity-dependent regulation of h channel distribution in hippocampal CA1 pyramidal neurons. J Biol Chem 282:33168–33180.

Shin M, Simkin D, Suyeoka GM, Chetkovich DM (2006) Evaluation of HCN2 abnormalities as a cause of juvenile audiogenic seizures in Black Swiss mice. Brain Res 1083:14–20.

Smith AJ, Owens S, Forsythe ID (2000) Characterisation of inhibitory and excitatory postsynaptic currents of the rat medial superior olive. J Physiol 529:681–698.

Stuart G, Spruston N (1998) Determinants of voltage attenuation in neocortical pyramidal neuron dendrites. J Neurosci 18:3501–3510.

Surges R, Brewster AL, Bender RA, Beck H, Feuerstein TJ, Baram TZ (2006) Regulated expression of HCN channels and cAMP levels shape the properties of the h current in developing rat hippocampus. Eur J Neurosci 24:94–104.

Svirskis G, Kotak V, Sanes DH, Rinzel J (2002) Enhancement of signal-to-noise ratio and phase locking for small inputs by a low-threshold outward current in auditory neurons. J Neurosci 22:11019–11025.

Svirskis G, Kotak V, Sanes DH, Rinzel J (2004) Sodium along with low-threshold potassium currents enhance coincidence detection of subthreshold noisy signals in MSO neurons. J Neurophysiol 91:2465–2473.

Tang ZQ, Dinh EH, Shi W, Lu Y (2011) Ambient GABA-activated tonic inhibition sharpens auditory coincidence detection via a depolarizing shunting mechanism. J Neurosci 31:6121–6131.

Taschenberger H, von Gersdorff H (2000) Fine-tuning an auditory synapse for speed and fidelity: developmental changes in presynaptic waveform, EPSC kinetics, and synaptic plasticity. J Neurosci 20:9162–9173.

Ulens C, Tytgat J (2001) Functional heteromerization of HCN1 and HCN2 pacemaker channels. J Biol Chem 276:6069–6072.

Vasilyev DV, Barish ME (2002) Postnatal development of the hyperpolarization-activated excitatory current Ih in mouse hippocampal pyramidal neurons. J Neurosci 22:8992–9004.

Viscomi C, Altomare C, Bucchi A, Camatini E, Baruscotti M, Moroni A, DiFrancesco D (2001) C terminus-mediated control of voltage and cAMP gating of hyperpolarization-activated cyclic nucleotide-gated channels. J Biol Chem 276:29930–29934.

Wainger BJ, DeGennaro M, Santoro B, Siegelbaum SA, Tibbs GR (2001) Molecular mechanism of cAMP modulation of HCN pacemaker channels. Nature 411:805–810.

Yamada R, Kuba H, Ishii TM, Ohmori H (2005) Hyperpolarization-activated cyclic nucleotide-gated cation channels regulate auditory coincidence detection in nucleus laminaris of the chick. J Neurosci 25:8867–8877.

Yang L, Monsivais P, Rubel EW (1999) The superior olivary nucleus and its influence on nucleus laminaris: a source of inhibitory feedback for coincidence detection in the avian auditory brainstem. J Neurosci 19:2313–2325.

Yin TC, Chan JC (1990) Interaural time sensitivity in medial superior olive of cat. J Neurophysiol 64:465–488.

Yu HG, Lu Z, Pan Z, Cohen IS (2004) Tyrosine kinase inhibition differentially regulates heterologously expressed HCN channels. Pflugers Arch 447:392–400.

Zolles G, Klöcker N, Wenzel D, Weisser-Thomas J, Fleischmann BK, Roeper J, Fakler B (2006) Pacemaking by HCN channels requires interaction with phosphoinositides. Neuron 52:1027–1036.

Zong X, Eckert C, Yuan H, Wahl-Schott C, Abicht H, Fang L, Li R, Mistrik P, Gerstner A, Much B, Baumann L, Michalakis S, Zeng R, Chen Z, Biel M (2005) A novel mechanism of modulation of hyperpolarization-activated cyclic nucleotide-gated channels by Src kinase. J Biol Chem 280:34224–34232.